

Journal of Materials Chemistry C

Materials for optical, magnetic and electronic devices

Accepted Manuscript

This article can be cited before page numbers have been issued, to do this please use: G. Keyun, Z. Zhang, T. OHSAWA, M. Imura, J. Huang, Y. Koide and M. Liao, *J. Mater. Chem. C*, 2025, DOI: 10.1039/D4TC05169F.



This is an Accepted Manuscript, which has been through the Royal Society of Chemistry peer review process and has been accepted for publication.

Accepted Manuscripts are published online shortly after acceptance, before technical editing, formatting and proof reading. Using this free service, authors can make their results available to the community, in citable form, before we publish the edited article. We will replace this Accepted Manuscript with the edited and formatted Advance Article as soon as it is available.

You can find more information about Accepted Manuscripts in the [Information for Authors](#).

Please note that technical editing may introduce minor changes to the text and/or graphics, which may alter content. The journal's standard [Terms & Conditions](#) and the [Ethical guidelines](#) still apply. In no event shall the Royal Society of Chemistry be held responsible for any errors or omissions in this Accepted Manuscript or any consequences arising from the use of any information it contains.

ARTICLE

Photo-response performance regulation of type-Ib diamond-based photodetector by H₂ annealing and ozone treatmentKeyun Gu,^{a,b} Zilong Zhang,^b Takeo Ohsawa,^b Masataka Imura,^b Jian Huang,^{a*} Yasuo Koide,^b and Meiyong Liao^{b*}Received 00th January 20xx,
Accepted 00th January 20xx

DOI: 10.1039/x0xx00000x

Ultra-wide bandgap semiconductor diamond-based deep ultraviolet (DUV) photodetector (PD) has attracted extensive attention due to its immunity to solar light on the earth and thermal stability in extremely harsh environments. However, the preparation of high-quality and high-pure single-crystal diamond epilayer remains a major obstacle to achieve high photo-response performance. Here, we demonstrate that diamond PDs with tunable photoresponse properties can be obtained on type-Ib diamonds through simple annealing in H₂ ambient and surface ozone treatment process. The surface holes and the nitrogen defects inside the type-Ib diamond work together to regulate the overall photoresponse performance. The responsivity of the PDs can be adjusted from 84.3 A/W to 2.65×10⁴ A/W, and the response time can be modulated from 42.5 s to less than 240 ms. The achievement of photo response performance modulation of PDs originates from the cooperative effect of deep natural nitrogen defects and surface states. Thus, our new findings provide an alternative method and facile strategy for the tailoring of PDs' performance, which can meet different application requirements.

Introduction

Solar-blind deep-ultraviolet (DUV) photodetector exhibits excellent spectral selectivity since it responds to the light with wavelengths shorter than 280 nm, which is almost non-existent in the earth's atmosphere¹⁻³. The extremely low noise interference from environment enables high-accuracy detection of solar-blind DUV lights. Thus, the solar-blind DUV PDs are in demand for the applications covering intersatellite secure communications⁴, DUV imaging⁵, and environmental monitoring and analysis⁶⁻⁸. Diamond is a single-element ultra-wide bandgap (5.5 eV) semiconductor which has an excellent thermally and chemically stable structure, the highest thermal conductivity (22 W·cm⁻¹·K⁻¹), and a large breakdown field >10 MV/cm⁹⁻¹². Compared with multi-element compound semiconductors, such as AlGaIn, Ga₂O₃, and MgZnO, diamond does not have problems such as component segregation or oxygen vacancies¹³⁻¹⁶. Besides, diamond has high radiation resistance¹⁷, meaning it will not be damaged under long-term exposure to high-energy DUV light. Furthermore, diamond can achieve high sensitivity to DUV light but weak response to visible light, making it an extremely attractive material for preparing solar-blind DUV PDs.

The initial efforts in developing diamond PDs were mainly on polycrystalline diamond. In 1993, Binari *et al* fabricated a metal-semiconductor-metal (MSM) PD based on polycrystalline diamond, which showed a quantum efficiency of 39% at 400 V bias voltage and

under a wavelength of 200 nm¹⁸. In 1998, Jiang *et al* demonstrated a MSM PD based on diamond thin film grown on a silicon substrate, which achieved a low operating voltage around 5 V¹⁹. In 2005, we investigated the performance of PD based on boron (B)-doped homoepitaxial single-crystal diamond (SCD), which showed a high ultraviolet photocurrent at 220 nm (seven orders of magnitude higher than dark current) and a high spectral selectivity (DUV/visible rejection ratio of 10⁶)²⁰. Lin *et al* developed SCD MSM PDs, which showed a responsivity of 21.8 A/W and a detectivity of 1.39 × 10¹² cm Hz^{1/2} W⁻¹ at 218 nm light²¹. A responsivity of 524.9 A/W was later achieved by treating the SCD epitaxial layer with hydrogen plasma and optimizing the Schottky barrier with electrode contact²². Up to date, almost all high-performance diamond-based solar blind DUV PDs rely on high-quality epitaxial layers. Recently, we showed a EQE of 9.41×10⁶% for the diamond DUV PDs by simply treating a type-Ib diamond substrate using hydrogen plasma treatment²³. Regardless of the growth of high-quality epitaxial layers or hydrogen plasma treatment, MPCVD equipment was used in our previous work.

In this work, we report the development of DUV detectors by simply annealing commercial type-Ib diamond substrates in a H₂ ambient. By combining with UV/ozone treatment, the overall response properties such as the DUV responsivity, response speed, dark current, and spectral response of the diamond PDs can be regulated. The responsivity (R) of the PD based on hydrogen-annealed diamond is up to 2.65×10⁴ A/W, corresponding to an ultrahigh external quantum efficiency (EQE) of 1.50×10⁷ % but a lower response speed. After UV/ozone treatment, the device response time can be as short as less than 240 ms. The modulation of the photoresponse properties of the H-annealed type-Ib diamond is resulted from the cooperative effect of the nitrogen impurity in diamond and the surface states. These findings provide a simple and effective strategy for fabricating diamond DUV PDs, which can meet different application requirements.

^a School of Materials Science and Engineering, Shanghai University, Shanghai 200444, PR China.

Email: jianhuang@shu.edu.cn

^b Research Center for Functional Materials, National Institute for Materials Science (NIMS), Namiki 1-1, Tsukuba, Ibaraki 305-0044, Japan.

Email: meiyong.liao@nims.go.jp

† Electronic Supplementary Information (ESI) available. See DOI: 10.1039/x0xx00000x



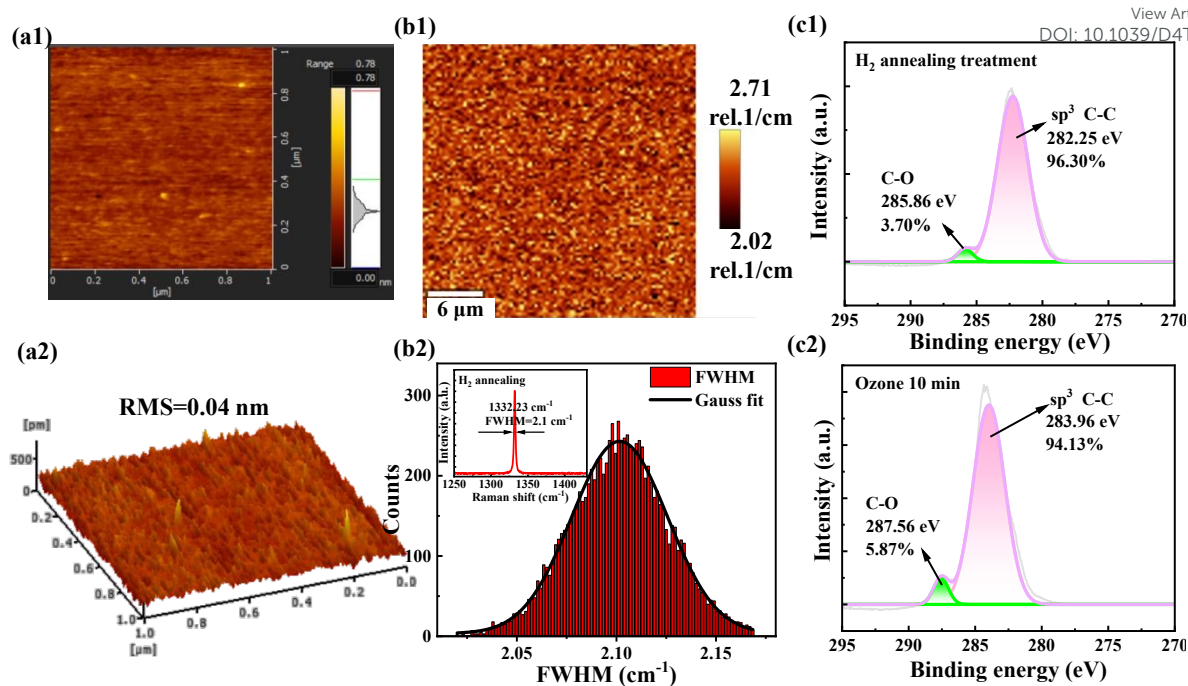


Fig. 1. (a1-a2) 2 dimension (D) and 3D surface morphology of H₂ annealed diamond. (b1-b2) Raman imaging of an area of 30x30 μm², and statistic distribution of the Raman FWHM of the H₂ annealed diamond. (c1-c2) X-ray photoelectron spectroscopy (XPS) spectra of H₂ annealed and 10 min ozone treated diamond.

Results and discussion

Material characterization

The surface morphology of the H₂ annealed typ-Ib diamond substrate scanned by AFM was shown in Figure 1(a1) and (a2). It can

be seen that the surface of diamond is smooth without large bulges or damage after H₂ annealing. The root mean square (RMS) is extremely low (~0.04 nm). Figure 1(b1-b2) display the 2D mapping of the Raman peak full width at half maximum (FWHM) of an area of 30x30 μm² and the statistical histogram, respectively. The Raman

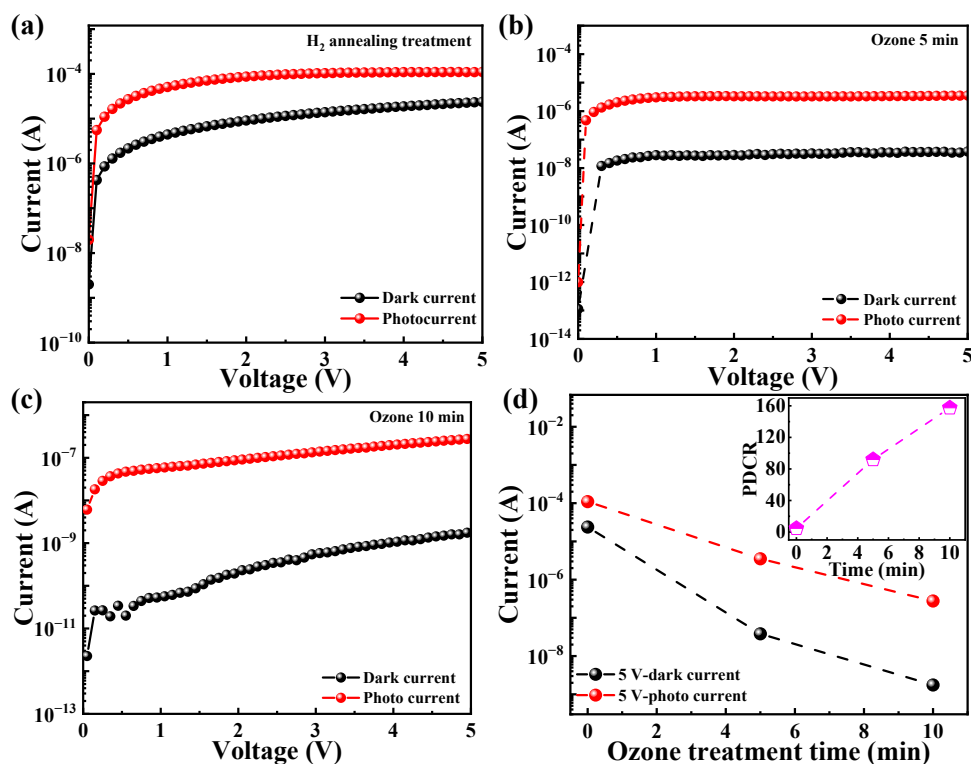


Fig. 2. I-V characteristics of the diamond PDs. (a) H₂-annealed, (b) Ozone treatment for 5 min (c) Ozone treatment for 10 min. (d) Dark and photo current vs ozone treatment time.



peak position is around 1332.23 cm^{-1} , which is close to the standard value of 1332.5 cm^{-1} . The FWHM is evenly distributed, and the average FWHM is around 2.1 cm^{-1} . Based on the XPS analysis shown in Figure 1(c1) and (c2), for hydrogen annealed diamond, the C-C sp^3 components accounts for 96.3% and C-O accounts for 3.7%. The peak of C-O is attributed to the surface adsorbed carbon oxides when exposure in ambient air^{24, 25}. After 10 min ozone treatment, the content of C-O increases to 5.87%, indicating its surface gradually changes from hydrogen terminal to oxygen terminal. Furthermore, the sp^3 C-C peak of ozone treated diamond shifts from 282.25 eV to 283.96 eV, which can be explained by the difference of band bending^{26, 27}.

Photoresponse properties regulation

The surface electrical conductivity of H-terminated diamond can be enhanced by hydrogen annealing. Taking into that the bulk type-Ib diamond contains a large amount of nitrogen (N) around 10^{19}cm^{-3} , the surface electrical conductivity caused by two-dimensional hole gas (2DHG) is decayed because of the depletion of partial surface holes due to N trapping, which is similar to hydrogen plasma treated surfaces. The as-annealed diamond-based PD has a dark current around $2.37 \times 10^{-5}\text{ A}$ at 5 V, as shown in Figure 2(a). This value is two order of magnitude lower than that of "intrinsic" diamond with surface H-termination²⁸. The dark current of the PD ozone treated for 5 minutes is reduced around $3.82 \times 10^{-8}\text{ A}$, and that of the PD ozone treated for 10 minutes is around $1.75 \times 10^{-9}\text{ A}$, as depicted in Figure 2(b) and (c), respectively. Under 220 nm DUV light illumination, the photocurrent of three PDs is enhanced to $1.10 \times 10^{-4}\text{ A}$, $3.51 \times 10^{-6}\text{ A}$, and $2.76 \times 10^{-7}\text{ A}$, respectively, illustrating a sensitive response to DUV light. The PD's dark current and photocurrent gradually decrease with the prolonged ozone treatment durations (Figure 2(d)), resulting from the decrease of 2DHG concentration. And the ratio of photocurrent to dark current (PDCR) of the PDs increases with the ozone treatment time.

The responsivity (R) and external quantum efficiency, EQE , critical figure-of-merits in photodetectors, representing the ratio of extracted carriers and incident photons, is obtained under 5 V bias. The responsivity, R , is calculated according to:

$$R = EQE \frac{e\lambda}{hc}$$

where e , λ , h , and c are electron charge, incident light wavelength, Planck constant, and light speed, respectively²⁹⁻³¹. The PDs exhibit higher EQE in DUV region and lower EQE in visible region. By using the optically active area of $5 \times 10^{-4}\text{ cm}^2$ and the power density ($6.50\text{ }\mu\text{W}/\text{cm}^2$) of the 220 nm light, the responsivity of $2.65 \times 10^4\text{ A/W}$ is obtained, corresponding to a EQE of $\sim 1.50 \times 10^7\%$ for the H_2 -annealed PD, as shown Figure 3. While the EQE of the PD with 5 min and 10 min UV/ozone treatments are $6.00 \times 10^5\%$ and $4.76 \times 10^4\%$, respectively, corresponding to the responsivity of $1.06 \times 10^3\text{ A/W}$ and 84.3 A/W , respectively. The cut-off wavelength shifts rightward to 270 nm because the presence of a large amount of nitrogen (N) doping inside HPHT diamond will enhance light absorption to promote photocurrent^{32, 33}. The detectivity, D^* , is determined by noise current I_n , responsivity R , illumination area A , and the bandwidth B ^{34, 35}, which is expressed by:

$$D^* = \frac{R\sqrt{AB}}{I_n}$$

The noise current of the H_2 annealed PD, the 5 min ozone-treated PD, the 10 min ozone-treated PD are $3.11 \times 10^{-7}\text{ A/Hz}^{1/2}$, $2.65 \times 10^{-9}\text{ A/Hz}^{1/2}$, and $3.09 \times 10^{-11}\text{ A/Hz}^{1/2}$, respectively, as illustrated in Figure 3(c). Based on the noise current, the D^* can be calculated to be $6.03 \times 10^9\text{ cm Hz}^{1/2}\text{ W}^{-1}$, $2.83 \times 10^{10}\text{ cm Hz}^{1/2}\text{ W}^{-1}$, and $1.93 \times 10^{11}\text{ cm Hz}^{1/2}\text{ W}^{-1}$ as for the H_2 annealed PD, the 5 min ozone-treated PD, the 10 min ozone-treated PD, respectively, as shown in Figure 3(d). The PD with 10 min ozone treatment has a higher D^* , attributing to the lower noise current. And all PDs exhibits higher D^* in DUV region.

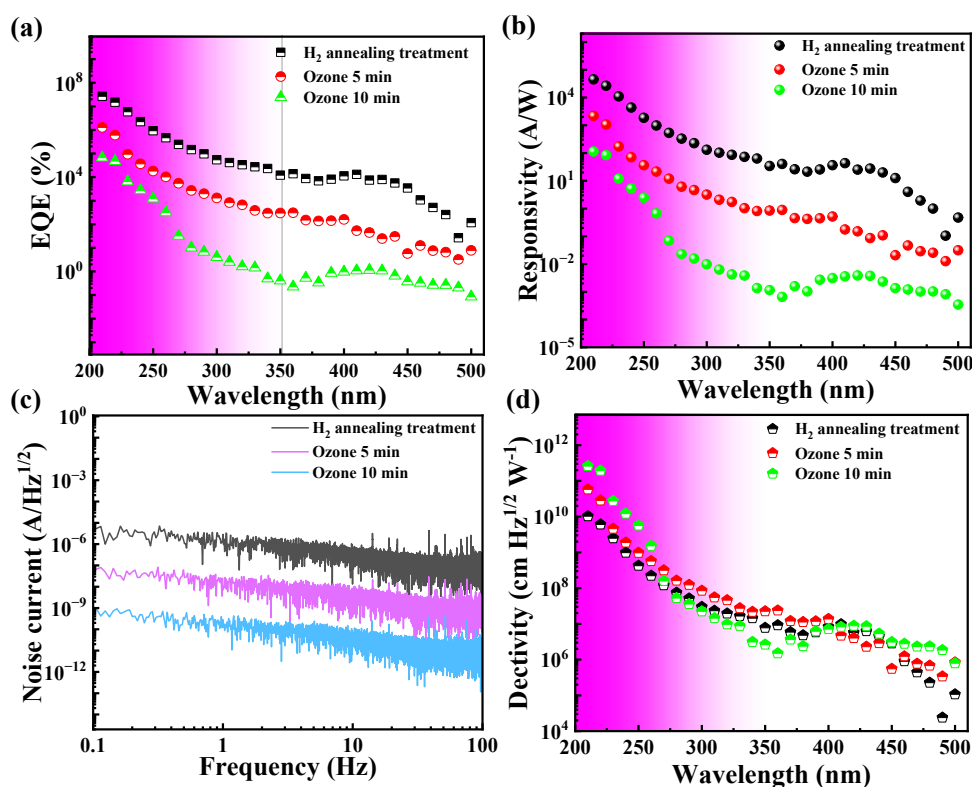


Fig. 3. (a) The measured external quantum efficiency, EQE , (b) responsivity, R , (c) noise current, and (d) detectivity, D^* of PDs.



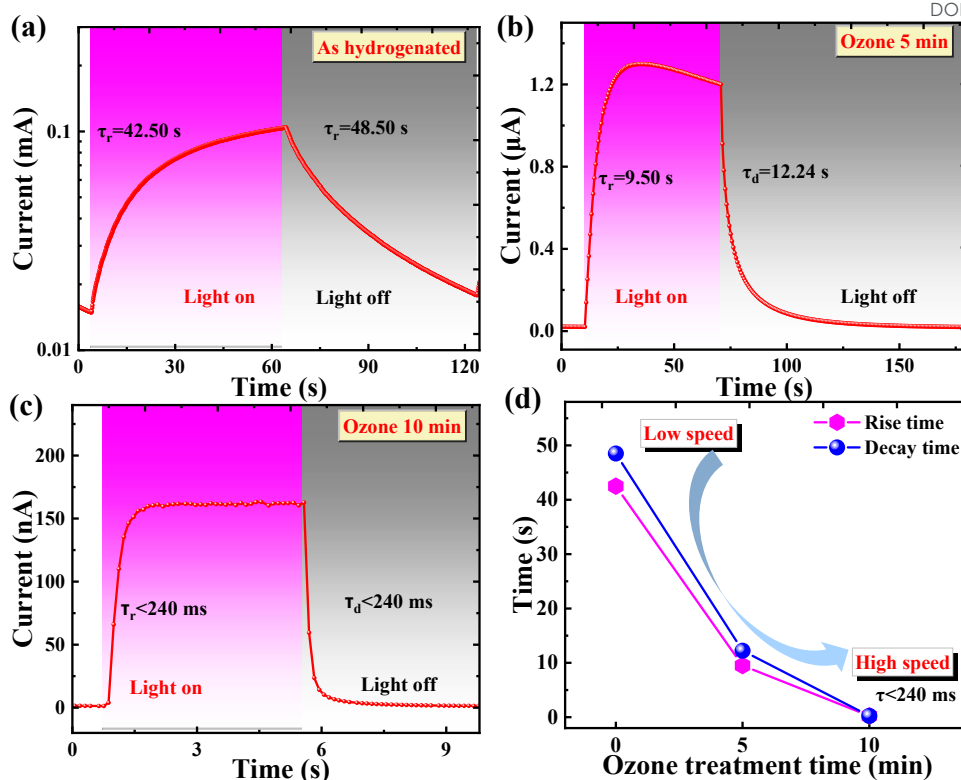


Fig. 4. Time-dependent photo-response of PDs. (a) H₂-annealed, (b) Ozone treated for 5 min (c) Ozone treated for 10 min. (d) Response time vs ozone treatment time.

Furthermore, the response time including the rise time τ_r (10% to 90% of the maximum photocurrent) and the decay time τ_d (90% to 10% of the maximum photocurrent) were calculated. The τ_r and τ_d of H₂ annealed PD are beyond 42 s (Figure 4(a)), and the response time becomes shorter with the prolong of ozone time (Figure 4(d)). The PDs with 5 min ozone and 10 min ozone treatment have the response time of $\tau_r/\tau_d=9.50$ s/12.24 s, and $\tau_r/\tau_d<240$ ms, respectively, as displayed in Figure 4(b) and Figure 4(c), respectively. The PDs show no current decay for cyclic switching, indicating that the PDs have good stability, as shown in Figure S2. Furthermore, the photocurrent increases linearly with the incident power density.

The key parameters including the dark current, R , EQE , and response time of diamond-based PDs in this work and previously reported^{22, 23, 36-42} are summarized in Table 1. Almost all other reported diamond PDs in the table are based on epitaxial SCD layers prepared using MPCVD method. Our another work²³ demonstrates an EQE of $9.41 \times 10^6\%$ by using MPCVD hydrogen plasma to treat a

type-Ib diamond surface. In this work, we simply used H₂ annealed commercial HPHT type-Ib diamond to achieve comparable ultrahigh responsivity (2.65×10^4 A/W) and external quantum efficiency ($1.50 \times 10^7\%$). Furthermore, the PDs in this work operates with a voltage as low as 5V and the response performance of the PDs can be tailored through surface treatments. The surface conductivities and photoresponse properties for the diamond surfaces either by hydrogen plasma treatment or thermal annealing in a hydrogen ambient are similar. The thermal stability of the diamond surfaces treated by these two methods are under investigation.

Photoresponse mechanism

Hydrogen-annealed type-Ib diamond shows a negative electron affinity (NEA) and exhibits surface conductivity due to the formation of two-dimensional hole gas on the surface⁴³⁻⁴⁵. Thus, the energy band of H₂ annealed diamond bends upwards. Furthermore, there are nitrogen defects inside the type Ib-diamond, which compensate surface holes electrons and results in an increase in ionized N⁺ traps,

Table 1. Comparisons of photodetection performances of Ga₂O₃-based photodetectors.

Material	Structure	Dark current	Responsivity (A/W)	EQE (%)	Response time(τ_r/τ_d)	Ref.
B-doped SCD	MSM	10^{-12} A@30 V	18@-23 V, 220 nm	1.01×10^4	<10ms	34
SCD	MSM	1.12×10^{-12} A@30 V	0.20@30 V, 220 nm	1.12×10^2	20 μ s/1000 μ s	35
Graphene-MCD	Heterojunction	10^{-6} A/cm ²	1.4@5 V, 220 nm	7.9×10^2	-	36
SCD	MSM	10^{-12} A@30 V	1.18@50 V, 210 nm	6.66×10^2	640 ms/34 ms	37
SCD	MSM	10^{-13} A@50 V	0.11@7 V, 220 nm	62.1	-	38
SCD	MSM	1.08×10^{-10} A@13 V	524.9@13 V, 220 nm	2.96×10^5	0.16 μ s/120 μ s	20
SCD	MSM	10^{-12} A@47 V	0.013@47 V, 225 nm	7.19	5ns/20ns	39
SCD	MSM	10^{-12} A@30 V	0.325@30 V, 210 nm	1.92×10^2	1.2 ms	40
H-plasma treated Ib-diamond	MSM	2.34×10^{-5} A@5 V	1.6×10^4 @5 V, 220 nm	9.41×10^6	30.4 s	21
H ₂ annealed Ib-diamond	MSM	2.37×10^{-5} A@5 V	2.65×10^4 @5 V, 220 nm	1.50×10^7	42.5 s/48.5 s	This work
Ozone 5 min Ib-diamond	MSM	3.82×10^{-8} A@5 V	1.06×10^3 @5 V, 220 nm	6.00×10^5	9.50 s/12.24 s	This work
Ozone 10 min Ib-diamond	MSM	1.75×10^{-9} A@5 V	84.3@5 V, 220 nm	4.76×10^4	<240 ms	This work



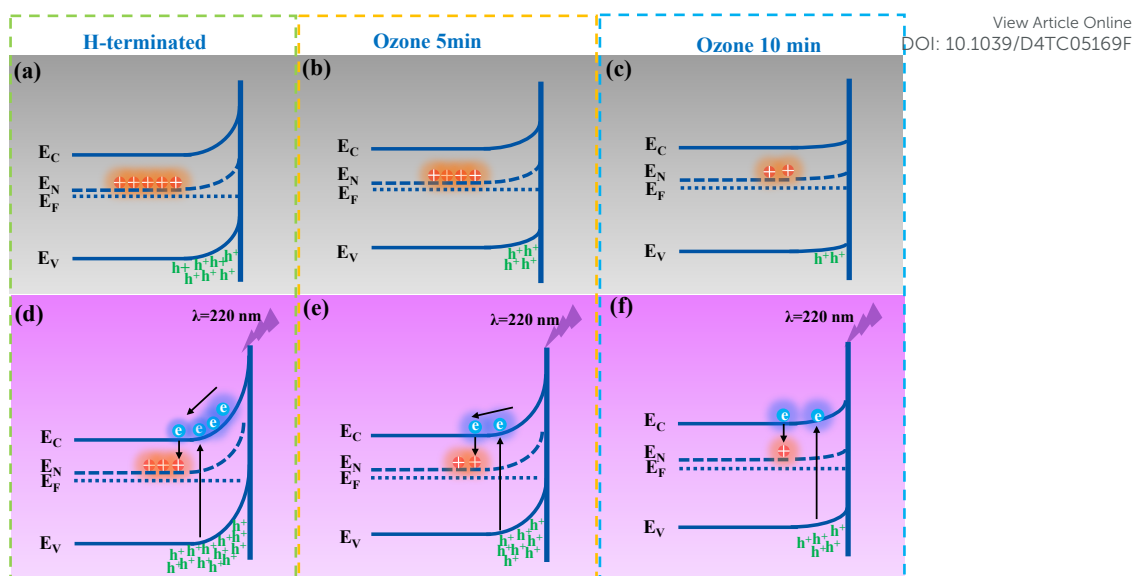


Fig. 5. Energy band diagrams of H₂-annealed, ozone-treated 5 min, and ozone-treated 10 min PDs: (a), (b), and (c) in the dark condition and (d), (e), and (f) under the 220 nm UV light.

as shown in Figure 5(a). This results in the H₂-annealed type-Ib diamond PD possessing lower dark current (2.37×10^{-5} A) than those of H-terminated intrinsic diamonds (\sim mA)^{46, 47}. After ozone treatment, the surface conductivity and surface holes concentration decrease, the energy band bends upward slightly, and less nitrogen is ionized, as shown in Figure 5(b) and (c). Under DUV light illumination, the electrons in the valence band are excited to the conduction band, and some of the electrons are captured by N⁺ traps, causing equivalent holes to accumulate near the surface and the energy band bending upward more sharply, as shown in Figure 5(d). This corresponds to the ultrahigh EQE ($1.50 \times 10^7\%$) and responsivity (2.65×10^4 A/W). While the regulation process of more N⁺ traps slow down the overall carrier recombination process, so the response time of the H₂-annealed type-Ib diamond PD is longer ($\tau_r/\tau_d = 42.50$ s/48.50 s). As the UV/ozone treatment time increases, surface holes and N⁺ traps decrease, as depicted in Figure 5(e) and (f), resulting in the lower EQE of $6.00 \times 10^5\%$ and $4.76 \times 10^4\%$, respectively for the 5min and 10 min ozone treated PDs. And the carrier recombination gradually changes from being dominated by N⁺ traps to being dominated by band-to-band. Therefore, the response speed accelerates ($\tau_r/\tau_d < 240$ ms for 10 min ozone treated PD).

Experimental

The type Ib-typed diamond with the dimensions of 2.5 mm \times 2.5 mm \times 0.5 mm was cleaned ultrasonically in acetone, absolute ethanol, and deionized water for 5 minutes, respectively. Before annealing in a H₂ ambient, the diamond substrate was boiled in an acid mixture of H₂SO₄ and HNO₃. The overall experimental treatment route is shown in Figure 6. The cleaned diamond was transferred to a high-vacuum chamber which has a base pressure of 10^{-7} Torr. The annealing temperature, the pressure, and the duration were, 860°C, 80 Torr, 1h, respectively. The Ti/Au interdigitated electrodes with a finger width 10 μ m were deposited on hydrogen annealed diamond surface. The optically active receiving area is around 5×10^{-4} cm². The as-annealed PDs were placed into an UV/ozone reaction chamber for 5 min and 10 min treatments. The optical image of the PD is shown in Figure S1. The diamond surface morphology and root mean square were characterized by an atomic force microscopy (AFM). The Raman spectrometer with a 532 nm laser was used to measure the crystal quality of the as-annealed diamond. A commercial X-ray photoelectron spectrometer (XPS, Thermo Fisher Scientific, Japan) was used to measure the binding states of the surface composition. The overall photoelectric performance of the PDs was measured by

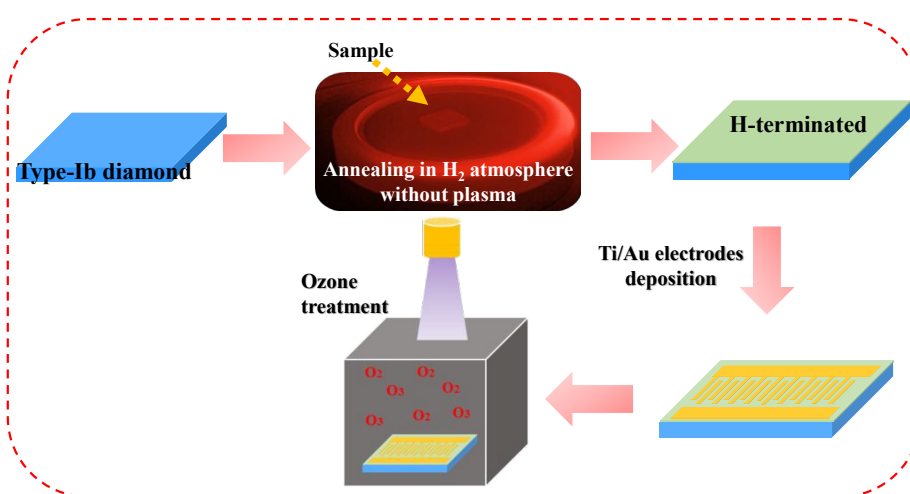


Fig. 6. Schematic diagrams of the experimental treatment route.



ARTICLE

Journal of Materials Chemistry C

using Keithley 2400 semiconductor Analyzer and an Ushio Xenon lamp combined with an Acton monochromator with order sorting filters and a standard lock-in amplifier technique. The power density of the 220 nm incident light is around 6.5 $\mu\text{W}/\text{cm}^2$.

Conclusions

In conclusion, a high-temperature annealing procedure in H_2 ambient was conducted to fabricate H-terminated type-Ib diamond-based PD. The surface characteristics and the overall photoresponse performance of H_2 annealed type-Ib diamond are comparable with those of hydrogen plasma-treated type-Ib diamond. The UV/ozone surface treatment regulated the photoresponse performance through the cooperation of surface states and the natural doped nitrogen in type Ib diamond. The responsivity was modulated from 2.65×10^4 A/W to 84.3 A/W and the response time from 42.5 s to <240 ms. These findings provide a simple and effective technique to fabricate DUV-PDs with tunable performance for different industrial applications.

Data availability

The authors confirm that the data supporting this article have been included in the article or supplementary Information.

Conflicts of interest

The authors declare that they have no conflict of interest.

Acknowledgements

This work was supported by JSPS KAKENHI (Grant Number 24H00287, 22K18957, 20H02212), Bilateral joint research between JSPS/CAS, and Advanced Research Infrastructure for Materials and Nanotechnology in Japan (ARIM) of MEXT (JPMXP1223NM5297). Keyun Gu thanked to the financial support from China Scholarship Council (No. 202306890007).

Notes and references

- X. Chen, K. Liu, Z. Zhang, C. Wang, B. Li, H. Zhao, D. Zhao, D. Shen, *ACS Appl. Mater. Interfaces*, 2016, 8, 4185-4191.
- T. Oshima, T. Okuno, N. Arai, N. Suzuki, H. Hino and S. Fujita, *Jpn. J. Appl. Phys.*, 2009, 48, 011605.
- Z. Zhang, C. Lin, X. Yang, Y. Tian, C. Gao, K. Li, J. Zang, X. Yang, L. Dong and C. Shan, *Carbon*, 2021, 173, 427-432.
- C. Lin, Y. Lu, Y. Tian, C. Gao, M. Fan, X. Yang, L. Dong and C. Shan, *Opt. Express*, 2019, 27, 29962-29971.
- Y. Chen, Y. Lu, C. Lin, Y. Tian, C. Gao, L. Dong and C. Shan, *J. Mater. Chem. C*, 2018, 6, 5727-5732.
- J. Chen, W. Ouyang, W. Yang, J. H. He and X. Fang, *Adv. Funct. Mater.*, 2020, 30, 1909909.
- C. Wu, F. Wu, C. Ma, S. Li, A. Liu, X. Yang, Y. Chen, J. Wang and D. Guo, *Mater. Today Phys.*, 2022, 23, 100643.
- C. Wu, F. Wu, H. Hu, S. Wang, A. Liu and D. Guo, *Mater. Today Phys.*, 2022, 28, 100883.
- M. Liao, L. Sang, H. Sun, T. Li and S. Koizumi, *Appl. Phys. Lett.*, 2021, 119, 119159.
- M. Liao, *Funct. Diam.*, 2022, 1, 29-46.
- C. E. Nebel, *Funct. Diam.*, 2023, 3, 2201592.
- K. Gu, Z. Zhang, G. Chen, J. Huang, Y. Koide, S. Koizumi, W. Zhao and M. Liao, *Carbon*, 2024, 225, 119159.
- D. Guo, Q. Guo, Z. Chen, Z. Wu, P. Li and W. J. Tang, *Mater. Today Phys.*, 2019, 11, 100157.
- Y. Chen, Y. Lu, X. Yang, S. Li, K. Li, X. Chen, Z. Xu, J. Zang and C. Shan, *Mater. Today Phys.*, 2021, 18, 100369.
- D. Thapa, J. Huso, K. Miklos, P. M. Wojcik, D. N. McIlroy, J. L. Morrison, C. Corolewski, M. D. McCluskey, T. J. Williams and M. Grant Norton, *J. Mater. Sci.: Mater. Electron.*, 2017, 28, 2511-2520.
- F. C. Massabuau, S. L. Rhode, M. K. Horton, T. J. O'Hanlon, A. Kovács, M. S. Zielinski, M. J. Kappers, R. E. Dunin-Borkowski, C. J. Humphreys and R. A. Oliver, *Nano Lett.*, 2017, 17, 4846-4852.
- J. Xu, J. Dai, F. Ren, Y. Wang, P. Wang, S. Xu, S. Wu, J. Lin, Y. Yang and D. Guo, *Carbon*, 2021, 182, 525-536.
- S. Binari, M. Marchywka, D. Koolbeck, H. Dietrich, D. Moses, *Diam. Relat. Mater.*, 1993, 2, 1020-1023.
- W. Jiang, J. Ahn, F. Xu, C. Liaw, Y. Chan, Y. Zhou and Y.-L. Lam, *Appl. Phys. Lett.*, 1998, 72, 1131-1133.
- J. Alvarez, M. Liao and Y. Koide, *Appl. Phys. Lett.*, 2005, 87, 2101-2103.
- C. N. Lin, Y. J. Lu, X. Yang, Y. Z. Tian, C. J. Gao, J. L. Sun, L. Dong, F. Zhong, W. D. Hu and C. X. Shan, *Adv. Opt. Mater.*, 2018, 6, 1800068.
- C. Lin, Z. Zhang, Y. Lu, X. Yang, Y. Zhang, X. Li, J. Zang, X. Pang, L. Dong and C. Shan, *Carbon*, 2022, 200, 510-516.
- K. Gu, Z. Zhang, G. Chen, L. Sang, J. Huang, Y. Koide and M. Liao, *The 19th IEEE NEMS*, 2024, pp. 1-4.
- T. Hattori, T. Igarashi, M. Ohi and H. Yamagishi, *Jpn. J. Appl. Phys.*, 1989, 28, L1436.
- M. Kubovic, M. Kasu, H. Kageshima, F. J. D. Maeda and r. materials, *Diam. Relat. Mater.*, 2010, 19, 889-893.
- D. Ballutaud, N. Simon, H. Girard, E. Rzepka, B. Bouchet-Fabre, *Diam. Relat. Mater.*, 2006, 15, 716-719.
- M. Wang, N. Simon, G. Charrier, M. Bouttemy, A. Etcheberry, M. Li, R. Boukherroub and S. Szunerits, *Electrochem. Commun.*, 2010, 12, 351-354.
- M. Yuanchen, R. Zeyang, Y. Shiqi, S. Kai, Z. Jinfeng, Y. Xiaoli, N. Xiuxiu, Z. Jincheng and H. Yue, *Funct. Diam.*, 2023, 3, 2219687.
- Y. Xu and Q. Lin, *Appl. Phys. Rev.*, 2020, 7, 031301.
- G. Zeng, M. Zhang, Y. Chen, X. Li, D. Chen, C. Shi, X. Zhao, N. Chen, T. Wang and D. Zhang, *Mater. Today Phys.*, 2023, 33, 101042.
- Y. Qin, L. Li, X. Zhao, G. S. Tompa, H. Dong, G. Jian, Q. He, P. Tan, X. Hou and Z. Zhang, *Acs Photonics*, 2020, 7, 812-820.
- W. Kaiser and W. Bond, *Phys. Rev.*, 1959, 115, 857.
- V. Ralchenko, S. Pimenov, V. Konov, A. Khomich, A. Saveliev, A. Popovich, I. Vlasov, E. Zavedeev, A. Bozhko, E. Loubnin R. Khmel'nitskii, *Diam. Relat. Mater.*, 2007, 16, 2067-2073.
- Y. Fang, F. Guo, Z. Xiao and J. Huang, *Adv. Opt. Mater.*, 2014, 2, 348-353.
- C. Bao, Z. Chen, Y. Fang, H. Wei, Y. Deng, X. Xiao, L. Li and J. Huang, *Adv. Mater.*, 2017, 29, 1703209.
- M. Liao, Y. Koide and J. Alvarez, *Appl. Phys. Lett.*, 2007, 90, 071101.
- Z. Liu, F. Li, S. Li, C. Hu, W. Wang, F. Wang, F. Lin and H. Wang, *Sci. Rep.*, 2015, 5, 14420.
- M. Wei, K. Yao, Y. Liu, C. Yang, X. Zang and L. Lin, *Small*, 2017, 13, 1701328.



39. Z. Liu, D. Zhao, J. Ao, X. Chang, Y. Wang, J. Fu, M. Zhang and H. Wang, *Opt. Express*, 2018, 26, 17092-17098.
40. T. Teraji, S. Yoshizaki, H. Wada, M. Hamada, T. Ito, *Diam. Relat. Mater.*, 2004, 13, 858-862.
41. M. Girolami, V. Serpente, M. Mastellone, M. Tardocchi, M. Rebai, Q. Xiu, J. Liu, Z. Sun, Y. Zhao and V. Valentini, *Carbon*, 2022, 189, 27-36.
42. Y. Iwakaji, M. Kanasugi, O. Maida and T. Ito, *Appl. Phys. Lett.*, 2009, 94.
43. P. Zhang, S. Zhang, W. Chen, S. Yan, W. Ma and H. Wang, *Coatings*, 2020, 10, 876.
44. V. Seshan, D. Ullien, A. Castellanos-Gomez, S. Sachdeva, D. Murthy, T. Savenije, H. A. Ahmad, T. Nunney, S. Janssens and K. Haenen, *J. Chem. Phys.*, 2013, 138.
45. K. Gu, K. Wu, Z. Zhang, T. Ohsawa, J. Huang, Y. Koide, M. Toda and M. Liao, *Adv. Funct. Mater.*, 2024, 2420238.
46. W. Hu, X. Yu, T. Tao, K. Chen, Y. Ye, J. Zhou, Z. Xie, Y. Yan, B. Liu and R. Zhang, *Crystals*, 2023, 13, 1221.
47. Y. Huang, J. Xiao, R. Tao, Z. Liu, Y. Mo, X. Yu, Z. Cao, Y. Wu, Z. Li and H. Wang, *Appl. Phys. Lett.*, 2023, 123.

View Article Online
DOI: 10.1039/D4TC05169F

Open Access Article. Published on 13 February 2025. Downloaded on 2/22/2025 5:00:06 AM.
This article is licensed under a Creative Commons Attribution-NonCommercial 3.0 Unported Licence.



The authors confirm that the data supporting this article have been included in the article or supplementary Information.

